DOI: 10.30511/pcdp.2026.2089258.1077 - ISSN: 3060-8376 - Vol 3(3), 2026

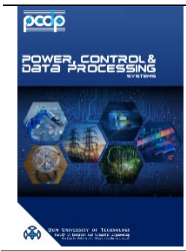


POWER, CONTROL AND DATA PROCESSING SYSTEMS

Available Online at: https://pcdp.qut.ac.ir/

# Sustainable Energy Management in Hybrid Multi-energy Systems: A Multi-Attribute Decision Making Model

**ARTICLE INFO**

***Article Type***
Original Research

***Authors***
Hamid Karimi[1,*]
Hamid Reza Sezavar[1]
Mohamad Kamarol Mohd Jamil[2]

[1] Department of electrical and computer engineering, Qom University of Technology, Qom, Iran.
[2] School of Electrical and Electronic Engineering, Universiti Sains Malaysia, Pulau Pinang, Malaysia.

Karimi.h@qut.ac.ir,
sezavar@qut.ac.ir,
eekamarol@usm.my,

**** Correspondence***
*Address*: Department of electrical and computer engineering, Qom University of Technology, Khodakaram Boulevard, Qom, Iran.
*Phone*: 36169000
*Fax*: -
Karimi.h@qut.ac.ir

***Article History***
Received: May 21, 2026
Accepted: July 01, 2026
ePublished: September 01, 2026

**ABSTRACT**

This paper proposes a multi-objective optimization for the optimal energy scheduling of renewable-based energy system. The proposed model simultaneously considers both economic and environmental indices in the operation planning to present a comprehensive scheduling for the energy system. The studied energy system integrates the electrical, heating, and cooling sectors to increase the synergy, reliability, and flexibility of the renewable-based energy system. This integration improves the utilization of renewable energy system because the surplus generation of photovoltaic and wind energy can be converted to other forms of energy to supply the required heat and cooling energy of the system. In addition, Shannon entropy and multi-attribute utility theory (MAUT) are used to determine the relative importance of economic versus environmental criteria and to prioritize the solutions based on the operator's viewpoint. The proposed model is tested on a standard case study and the numerical results present that the proposed model improves the emission of greenhouse gases by 4.8 % compared to single objective optimization in the normal condition. Also, compared to the scenario where no demand response is present, the demand response programs decreases the operating cost of the multi-energy system by 2.47 %.

**Keywords:** multi-energy system; sector coupling; sustainable management; renewable energy system.

# 1 Introduction

The integration of different energy such as electricity, heat, and cooling, often referred to as sector coupling or multi-energy systems (MES), improves the efficiency, reliability, and sustainability of the distributed energy systems [1, 2]. This integration enables a flexible operation for the distribution networks because the surplus generation of photovoltaic and wind energy system can be converted to other forms of energy to increase the synergy [3, 4]. However, the scheduling and energy conversion among different carriers considering different technical constraints need a comprehensive optimization framework [5].

In recent years, different studies have been investigated the operation scheduling of multi-energy systems. In [6], a NSGA-III algorithm is presented to model the energy management of a MES considering the exergy and economic indices. The authors utilizes the TOPSIS method to rank the optimal Pareto solutions for the MES. Reference [7] studies the performance of an advanced compressed air energy storage system on the operation scheduling of a MES. The proposed model integrates the electrical, heating, and cooling sectors to supply different forms of energy demands. The authors in [8] incorporated the battery energy storage systems to the MES using the NSGA-II/RSM optimization framework. The proposed model simultaneously minimize battery temperature and maximize the energy efficiency.

A robust optimization has been developed in [9] to model the coordination among the electric vehicle charging stations and user aggregators using a Nash-Stackelberg game. The authors in [10] studied the performance of different uncertainty modeling on the operation scheduling of a MES. The authors in [11] developed a day-ahead energy management scheme to coordinate the operation scheduling of multi-area MES consist of residential homes. The proposed model considers a cloud energy storage and models the peer-to-peer energy trading in the system. Also, a conditional value-at-risk algorithm is developed to model the uncertainty of electricity prices. Reference [12] proposes a multi-objective optimization using NSGA-III algorithm to optimize the total cost and carbon capture in a MES. This study integrates the hydrogen system to the electricity section to increase the flexibility of the MES.

A multi-layer optimization model has been developed in [13] to present an economic and power quality-based energy management for MES. In this study, the electrical, heating, cooling, and water sectors are integrated together to supply the energy and fresh water for the customers. The first layer of the proposed model considers the uncertainty of renewable generation using stochastic approach. The second stage presents a multi-objective optimization to minimize optimizes the total cost and extracted water from the underground sources. Also, the last layer of the proposed model is responsible to investigate the power quality induces of the electricity network. In the proposed structure, the authors considered the desalination unit and water wells to provide the fresh water for the MES. The authors in [14] developed a bi-level approach to model the coordination of a virtual power plant MES with several microgrids in the distribution system. In the upper-level of the proposed model, the virtual power plant MES integrates the water and energy sectors to supply the required energy and water for microgrids aims to maximize its profit. At the lower level, the microgrids try to minimize their operating cost. To this end, the microgrids are able to form different coalitions and increase their bargaining powers. The authors in [15] utilizes a NSGA-II framework to present a multi-objectives optimization for a MES. The proposed model considered the cost of electricity, carbon emission, and other technical objectives in its scheduling. A robust and multi-time scale approach has been developed in [16] to study the energy management of a hydrogen-based MES. The energy management of an off-grid MES has been studied in [17]. The authors applied the multi-objective particle swarm optimization and NSGA-II algorithms to simultaneously optimize energy cost, power loss, and the excess energy penalty. Reference [18] present a day-ahead scheduling using robust multi-objective optimization algorithm for home MES to simultaneously minimize the operating cost and user discomfort. The proposed model considers the uncertainty of RES to provide a reliable scheduling for MES.

An improved particle swarm optimization (IPSO) algorithm has been developed in [19] for the optimal operation of the integrated energy system. However, the proposed model is not able to ensure the optimal economic scheduling for the system. The authors in [20] proposed an improved artificial bee colony algorithm for the operation scheduling of a smart MES home to minimize daily total cost. However, the carbon emission is not considered as the objective function of the proposed model.

In this paper, we propose a multi-objective optimization framework that incorporates the electrical, heat, and cooling system to supply various types of energy. In the proposed model, the MES incorporates different energy storage systems such as battery storage devices, heat storage, and cooling storage systems to increase the flexibility of the system in all of sectors. In the electrical section, the renewable energy sources, such as photovoltaic and wind energy, diesel generators, and combined heat and power (CHP) units are considered to generate the needed electricity. Also, the demand response programs (DRP) are implemented to enable the demand-side flexibility in the electricity section. In the heating section, the needed heat can be provided by CHP units and boiler. Also, the thermal DRP is develop to create the cost-saving opportunity in the heating section. In the cooling system, the absorption chiller, electric chiller, and ice storage conditioner can provide the required cooling energy for the MES. In the proposed model, the MES attempts to minimize the total cost and carbon emission simultaneously using normalized weighted sum approach. Also, the Shannon entropy method is used to determine the importance of the cost and carbon emission from the MES perspective. The normalized weighted sum approach finds the Pareto front solutions for the MES. Therefore, these solutions are ranked by the multi-attribute utility theory approach to define the appreciated operation from the system. The main contributions can be listed as follows:

1. Proposing a multi-objective optimization framework that considers both economic and carbon capture for the MES.
2. This paper presents a hybrid multi-objective decision making (MODM) and multi-attribute decision making (MADM) using weighted sum and multi-attribute utility theory approach to rank the optimal Pareto solutions.
3. The performance of the proposed model under emergency conditions are investigated.

## 2 Mathematical formulation of MES

This section presents the mathematical formulation of the objective functions and operational constraints of the MES.

### 2.1 Energy storage systems

Equations (1)-(6) present the formulation of different energy storage systems. The energy storage systems can increase the flexibility of the energy systems. When the generation of RES is more than electricity demand, the battery energy storage can be charged to store the surplus generation of RES. Also, when the generation of RES is less the forecasted values, the stored energy can be injected to the MES to compensate the RES shortage. Besides, the MES can convert the surplus generation of RES to other forms of energy to store it in the thermal and cooling energy system. This process increases the ability of MES to cover the uncertainty of RES and improves its flexibility.

$$SoC_{i,t} = SoC_{i,t-1} + (P_{i,t}^{ch}\eta^{i,ch}) - (\frac{P_{i,t}^{disch}}{\eta^{i,disch}}) \qquad (1)$$

$$SoC_i^{\min} \le SoC_{i,t} \le SoC_i^{\max} \qquad (2)$$

$$0 \le P_{i,t}^{ch} \le P_i^{ch,\max} E_{i,t}^{ch} \qquad (3)$$

$$0 \le P_{i,t}^{disch} \le P_i^{disch,\max} E_{i,t}^{disch} \qquad (4)$$

$$0 \le E_{i,t}^{ch} + E_{i,t}^{disch} \le 1 \qquad (5)$$

$$SoC_{i,1} = SoC_{i,24} \qquad (6)$$

Equation (1) shows the dynamic state of charge (SOC) of the energy storage systems. Equation (2) limits the SOC between the minimum and maximum bounds. Equations (3) and (4) limit the charging and discharging power of the energy storage systems, respectively. Equation (5) prevents simultaneous charging and discharging. Finally, Equation (6) shows that the initial and final energy should be the same.

### 2.2 Demand-side management

The MES performs both electrical and thermal demand response (DR) programs to increase demand-side flexibility in the electrical and heating sectors. Equations (7)-(10) present the general formulation of the DR programs.

$$0 \le P_{i,t}^{down} \le S_i^{down} D_{i,t} V_{i,t}^{down} \qquad (7)$$

$$0 \le P_{i,t}^{up} \le S_i^{up} D_{i,t} V_{i,t}^{up} \qquad (8)$$

$$\sum_t P_{i,t}^{up} = \sum_t P_{i,t}^{down} \qquad (9)$$

$$0 \le V_{i,t}^{up} + V_{i,t}^{down} \le 1 \qquad (10)$$

Equations (7) and (8) limit the downward and upward demand, respectively. Equation (9) shows that the upward and downward energy should be the same. Finally, Equation (10) does not allow the MES to simultaneously increase and decrease its demand.

### 2.3 Clean energy sources

Equations (11) and (12) represent the production of wind energy and photovoltaic, respectively.

$$P_t^{wt} = \begin{cases} 0, & V_t^{ac,wt} \le V^{ci,wt} \text{ or } V^{co,wt} \le V_t^{ac,wt} \\ P^{r,wt}\dfrac{V_t^{ac,wt} - V^{ci,wt}}{V^{rr,wt} - V^{ci,wt}}, & V^{ci,wt} \le V_t^{ac,wt} \le V^{rr,wt} \\ P^{r,wt}, & V^{rr,wt} \le V_t^{ac,wt} \le V^{co,wt} \end{cases} \qquad (11)$$

$$P_{t,s}^{pv} = B^{pv} A^{pv} I_{t,s}^{pv} (1 + N^{pv,mpt}(T^{pv,c} - T_t^{pv,out})) \qquad (12)$$

### 2.4 Combined heat and power unit

Equations (13)-(15) describe the operational constraints of CHP.

$$P_t^{e,chp} = G_t^{chp} LHV \eta^{e,chp} \qquad (13)$$

$$P_t^{h,chp} = G_t^{chp} LHV \eta^{h,chp} \qquad (14)$$

$$0 \le G_t^{chp} \le G_{\max}^{chp} \qquad (15)$$

Equations (13) and (14) show the output electricity and heat, respectively. Also, Equation (15) limits the natural gas imported to the CHP.

### 2.5 Operational constraints of boiler and gas turbine

Equations (16)-(19) model the operational constraints of the boiler and gas turbine units.

$$H_t^{boiler} = G_t^{boiler} LHV \eta^{boiler} \qquad (16)$$

$$0 \le H_t^{boiler} \le H_{\max}^{boiler} \qquad (17)$$

$$P_t^{DG} = G_t^{DG} LHV \eta^{DG} \qquad (18)$$

$$0 \le G_t^{boiler} \le G_{\max}^{boiler} \qquad (19)$$

$$0 \le G_t^{DG} \le G_{\max}^{DG} \qquad (20)$$

Equation (16) defines the heat generated by the boiler. Equation (17) limits the production of boiler. The electricity production of the gas turbine is determined by Equation (18). Finally, Equations (19) and (20) limit the natural gas input to the boiler and gas turbine, respectively.

## 2.6 Operational constraints of cooling sector

Equations (21)-(27) define the operational constraints of the cooling system.

$$P_{c,t}^{disch} = P_t^{ISC} COP^{ISC} \tag{21}$$

$$0 \le P_t^{ISC} \le P^{ISC,\max} \tag{22}$$

$$C_t^{EC} = P_t^{EC} COP^{EC} \tag{23}$$

$$0 \le P_t^{EC} \le P^{EC,\max} \tag{24}$$

$$C_t^{AC} = H_t^{AC} COP^{AC} \tag{25}$$

$$0 \le H_t^{AC} \le H^{AC,\max} \tag{26}$$

$$0 \le G_t^{boiler} + G_t^{chp} + G_t^{DG} \le p_{\max}^{gas} \tag{27}$$

Equation (21) presents the input energy to the cold storage. The electricity consumption of the ice storage conditioner is presented in Equation (22). The cooling generated by the electric chiller is formulated in Equation (23). Also, Equation (24) limits the electricity consumption of the electric chiller. Equation (25) calculates the cooling generated by the absorption chiller. Equation (26) limits the heat imported to the absorption chiller. Finally, Equation (27) limits the natural gas imported from the natural gas network.

## 2.7 Energy balance in MES

Equations (28)-(30) represents the electrical, heating, and cooling energy balance in the MES.

$$\begin{aligned} &P_t^{Grid} + P_t^{pv} + P_t^{wt} + P_t^{e,chp} + P_t^{DG} = \\ &D_t + (P_{e,t}^{up} - P_{e,t}^{down}) + (P_{e,t}^{ch} - P_{e,t}^{disch}) + P_t^{EC} \end{aligned} \tag{28}$$

$$\begin{aligned} &P_t^{h,chp} + H_t^{boiler} + P_{h,t}^{down} + P_{h,t}^{disch} \\ &= H_t^{demand} + P_{h,t}^{up} + P_{h,t}^{ch} + H_t^{AC} \end{aligned} \tag{29}$$

$$C_t^{ec} + C_t^{ac} + P_{c,t}^{disch} = C_t^{demand} \tag{30}$$

Equations (28)-(30) represent the electrical, heating, and cooling energy balances in the MES, respectively. Also, Eq. (31) limits the trading electricity by the main grid. Also, Eq. (32) limits the heat transfer of pipeline.

$$-P^{\max,grid} \le P_t^{Grid} \le P^{\max,grid} \tag{31}$$

$$\begin{aligned} &P_t^{h,chp} + H_t^{boiler} + P_{h,t}^{disch} \\ &\quad - P_{h,t}^{ch} - H_t^{AC} \le P^{h,\max} \end{aligned} \tag{32}$$

# 3 Objective function and optimization algorithm

In the proposed model, the MES attempts to simultaneously minimize the operating cost and carbon emission, respectively.

## 3.1 Objective functions of MES

The main objective function of the MES is to minimize its operating cost. This objective function is developed in Eqs. (33)-(39).

$$\begin{aligned} &\text{Minimize} \operatorname{Cos}t = \operatorname{Cos}t^{Grid} + \operatorname{Cos}t^{CHP} \\ &+ \operatorname{Cos}t^{boiler} + \operatorname{Cos}t^{EDR} + \operatorname{Cos}t^{HDR} + \operatorname{Cos}t^{DG} \end{aligned} \tag{33}$$

$$\operatorname{Cos}t^{Grid} = \sum_t P_t^{Grid} \pi_t^{Grid} \tag{34}$$

$$\operatorname{Cos}t^{CHP} = \sum_t G_t^{chp} \lambda_t^g \tag{35}$$

$$\operatorname{Cos}t^{boiler} = \sum_t G_t^{boiler} \lambda_t^g \tag{36}$$

$$\operatorname{Cos}t^{EDR} = \sum_t (C_{e,dr}^{down} P_{e,t}^{down} + C_{e,dr}^{up} P_{e,t}^{up}) \tag{37}$$

$$\operatorname{Cos}t^{HDR} = \sum_t (C_{h,dr}^{down} P_{h,t}^{down} + C_{h,dr}^{up} P_{h,t}^{up}) \tag{38}$$

$$\operatorname{Cos}t^{DG} = \sum_t G_t^{DG} \lambda_t^g \tag{39}$$

Equation (33) shows the total cost of the MES. The cost of energy trading with the main grid, generation cost of CHP, generation cost of boiler, electrical DR programs, thermal DR programs, and generation cost of gas turbine are presented in Eqs. (34)-(39), respectively.
The carbon emission is considered as the second objective function of the MES. This objective function is formulated in Eq. (40).

$$\begin{aligned} &\text{Minimize } Em = \sum_t U_{em}^g P_t^{Grid} \\ &\quad + \sum_t U_{em}^{chp} (P_t^{e,chp} + P_t^{h,chp}) \\ &\quad + \sum_t (U_{em}^{DG} P_t^{DG} + U_{em}^{boiler} P_t^{boiler}) \end{aligned} \tag{40}$$

To handle the multi-objective optimization, a normalized weighted sum approach is used to merge two conflict objective functions. The final objective function of the MES is formulated in Eq. (41):

$$\begin{aligned} &\text{Minimize } w^{\operatorname{Cos}t} \frac{\left|\operatorname{Cos}t - \operatorname{Cos}t^+\right|}{\left|\operatorname{Cos}t^+ - \operatorname{Cos}t^-\right|} \\ &\quad + w^{Em} \frac{\left|Em - Em^+\right|}{\left|Em^+ - Em^-\right|} \end{aligned} \tag{41}$$

Where $w^{\operatorname{Cos}t}$ and $w^{Em}$ determine the importance of two objective functions. Also, $\operatorname{Cos}t^+$ and $\operatorname{Cos}t^-$ are the ideal and non-ideal operating cost of the MES, respectively. Besides, $Em^{+}$ and $Em^{-}$ refer to the ideal and non-ideal carbon emission of the MES, respectively. By changing the weights of objective functions, different Pareto solutions are found.

## 3.2 Multi-attribute decision making

In order to rank different Pareto solutions, the multi-attribute decision making technique is used. At first, the Shannon entropy method is used to find the optimal weights of the objectives from the MES perspective. Also, the multi-attribute utility theory is utilized to rank th0e solutions.

- Shannon entropy method

The Shannon Entropy is a common method to define the weights of criteria in multi-criteria problems. It operates based on the degree of dispersion or uncertainty in each criterion. The greater the data dispersion for a criterion, the more information it conveys and the higher its weight. At first, the Shannon Entropy forms the decision matrix X as Eq. (42). Then, it normalized the decision matrix to form the normalized decision matrix P according to Eq. (43):

$$X = \left[ x_{ij} \right]_{n \times m} \tag{42}$$

$$P = \left[ p_{ij} \right]_{n \times m}, \quad p_{ij} = \frac{x_{ij}}{\sum_{i=1} x_{ij}} \tag{43}$$

At the next step, it calculates the entropy value for each criterion using Eq. (44).

$$E_j = -k \sum_{i=1}^{m} p_{ij}.Ln(p_{ij}), \quad k = \frac{1}{Ln(m)} \tag{44}$$

Using the entropy values, this approach calculates the degree of diversity as Eq. (45):

$$d_j = 1 - E_j \tag{45}$$

Finally, the weight of each objective function is determined by Eq. (46).

$$w_j = \frac{d_j}{\sum_{k=1}^{n} d_j} \tag{46}$$

- Multi-attribute utility theory

After determining the weight of objective functions, the multi-attribute utility theory (MAUT) is used to rank the Pareto solutions. The MAUT is a classical method and provides a utility for different solutions. At first, the MAUT defines the decision matrix X based on Eq. (43). At the second step, it constructs individual utility functions for each criterion based on Eqs. (47) and (48).

$$U_j(x_{ij}) = \frac{x_{ij} - x_j^{\min}}{x_j^{\max} - x_j^{\min}} \quad (\text{for benefit criteria}) \tag{47}$$

$$U_j(x_{ij}) = \frac{x_j^{\max} - x_{ij}}{x_j^{\max} - x_j^{\min}} \quad (\text{for cost criteria}) \tag{48}$$

Finally, Eq. (49) calculates the final utility of each alternative and the best option has the higher utility from the MES perspective.

$$U(A_i) = \sum_j w_j.U_j(x_{ij}) \tag{49}$$

Alternatives are ranked based on $U(A_i)$. The alternative with the highest $U(A_i)$ is the most preferred.

# 4 Simulation results and analysis

The proposed model is tested on a standard MES consist of electrical, heating, and cooling sectors. The electrical and thermal efficiency coefficients of CHP unit are 0.35 and 0.4, respectively. The maximum allowable input natural gas to the CHP unit is considered 300 m$^3$/h. The maximum allowable input natural gas to the boiler is 200 m3/h. The MES is operated in the grid-connected mode and the maximum electricity trading with the main grid is 2000 kW at each time slot. The cut-out, rated, and cut-in speeds of wind turbine model are 27 m/s, 15 m/s, and 4.5 m/s. The maximum generating power of gas turbine is 220 kW. Figures 1-3 show the load demands, electricity prices, and RES generation, respectively.

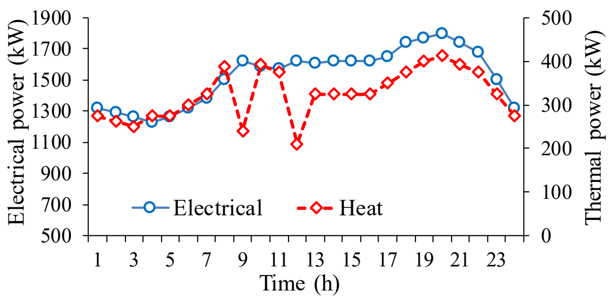


Fig. 1: Electrical and heating loads

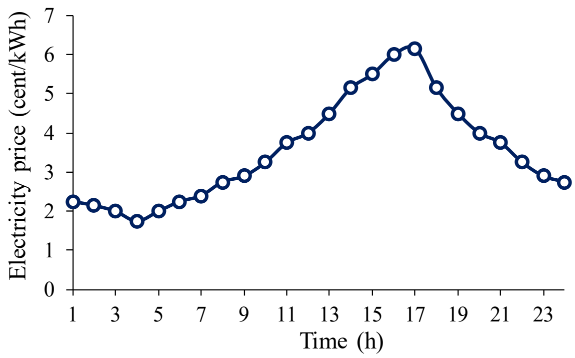


Fig: 2 Daily electricity prices

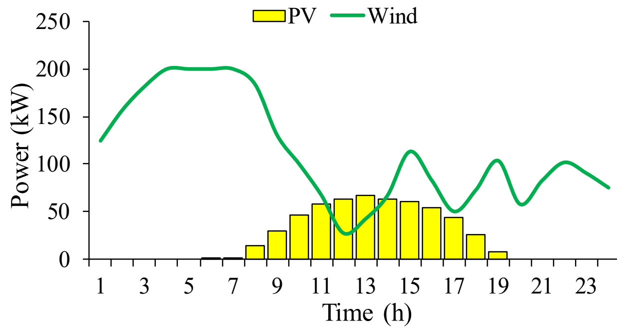


Fig. 3: Generation of renewable energy sources

The capacity of the battery energy storage system is 200 kWh. The charging and discharging efficiency of the battery energy storage system is considered 96 %. The charging and discharging powers of the battery energy storage system are considered 40 kW. The maximum purchased gas from gas network is 3400 $m^3$/h. The charging and discharging efficiency of the cooling storage is 0.97 and 0.95, respectively. The coefficients performance of absorption and electric chillers are 1.2 and 4, respectively.

Figure 4 shows the Pareto front for the MES. Also, Table 1 presents the operating cost and carbon emission of the MES for different weights.

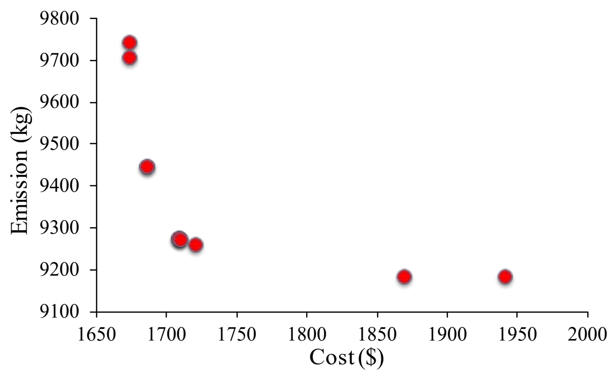


Fig. 4: Pareto front between cost and emission

Table 1: Pareto optimal solution of MES

| Options | $w_{cost}$ | $w_{emission}$ | Cost ($) | Emission (kg) | Rank |
|---|---|---|---|---|---|
| P1 | 1 | 0 | 1673.87 | 9740.947 | 6 |
| P2 | 0.9 | 0.1 | 1674.55 | 9705.717 | 5 |
| P3 | 0.8 | 0.2 | 1686.61 | 9446.339 | 3 |
| P4 | 0.7 | 0.3 | 1686.61 | 9446.339 | 3 |
| P5 | 0.6 | 0.4 | 1709.33 | 9272.653 | 1 |
| P6 | 0.5 | 0.5 | 1709.33 | 9272.653 | 1 |
| P7 | 0.4 | 0.6 | 1709.33 | 9272.653 | 1 |
| P8 | 0.3 | 0.7 | 1710.16 | 9271.236 | 2 |
| P9 | 0.2 | 0.8 | 1721.07 | 9259.374 | 4 |
| P10 | 0.1 | 0.9 | 1869.88 | 9181.783 | 7 |
| P11 | 0 | 1 | 1941.44 | 9180.715 | 8 |

Figure 4 presents the Pareto front for the MES. Table 1 ranks the Pareto solutions using Shannon entropy and multi-attribute utility theory. A closer inspection shows that solutions P5 through P7 exhibit identical performance and are each assigned rank 1. In fact, P5–P7 are weak Pareto solutions. According to Table 1, the operating cost and carbon emission of the best solution is $ 1709.33 and 9272.65 kg, respectively. Figure 5 shows the electricity trading among the main grid and MES.

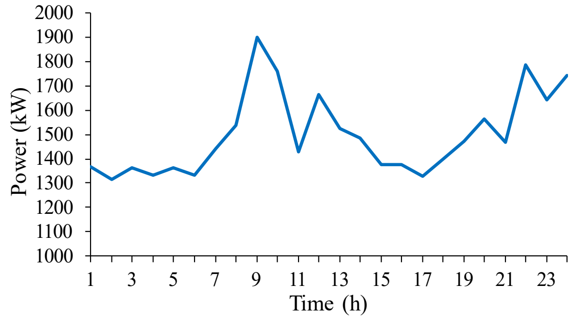


Figure 5: electricity trading between the main grid and MES

According to Fig. 5, the MES imports the maximum electricity during hours 8-11 because the market prices are less than the operating cost of local resources. Besides, during hours 14-20, the MES decreases its imported electricity from the main grid due to the higher electricity prices. Figure 6 presents the generated electricity by CHP unit.

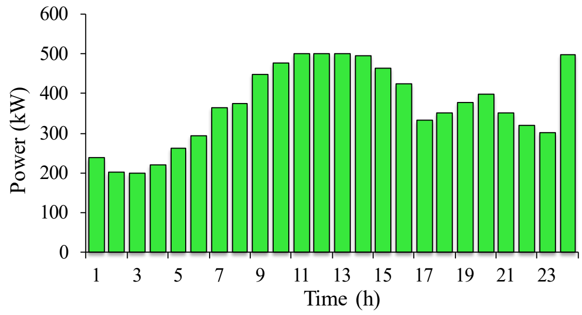


Figure 6: electricity generation by CHP

According to Fig. 6, the MES increases the generated electricity during 8-11 to supply the required electrical demand. Also, during hours 20-23, the MES decreases the generation of the CHP unit to supply the required electricity from the main grid due to lower electricity prices. Figure 7 shows the charging and discharging power of the battery storage system.

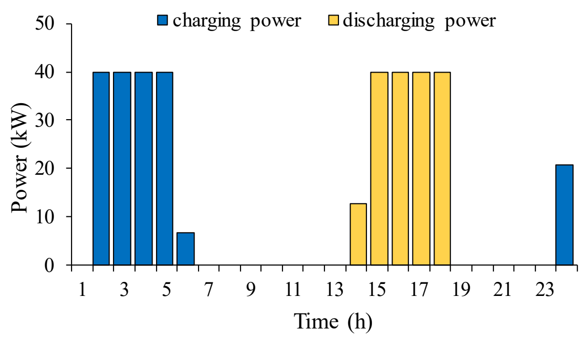


Figure 7: charging and discharging of battery storage system

According to Fig. 7, the MES charges the battery storage system during hours 2-6 and injects the stored electricity to the system during 14-18. During hours 2-6, the MES can purchase the electricity at lower prices and charges the battery storage system. Since the electricity prices during 14-18 are high, the MES injects the stored electricity to the system to decreases the operating cost. Figure 8 presents the output heat of boiler.

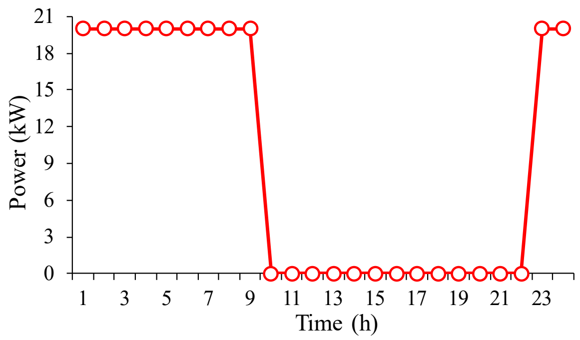


Figure 8: output heat of boiler

According to Fig.8, the MES only operates the boiler during hours 1-9 and 23-24. Actually, the MES supplies the required heat energy by CHP unit and the boiler is only operated when it is needed to help the MES. Since at the beginning of the day, most of the electricity is supplied by the main grid, and the CHP power generation is low, the heat produced by it is therefore minimal. As a result, a boiler is needed to supply heat during the early hours of the day.

Tables 2 and 3 presents impact of RES penetration on the performance of the MES. The PV penetration is changed from 0 % to 100% compared to the base case and the numerical results are presented in Table 2. It can be seen that by increasing the PV penetration from 0% to 100%, the operating cost of the MES is reduced from $ 1734.05 to $ 1709.32. Since the PV resources are not used any fossil fuel for their generation, their penetration decreases both operating cost and carbon emission. However, if the penetration of PV rescues decreases to 0%, the carbon emission has been increased by 100.29 kg. The carbon emission is increased because the MES should compensate this shortage by the main grid and CHP unit.

Table 2: Operating cost and carbon emission in different PV penetration

| Penetration (%) | Cost ($) | Carbon emission (kg) |
|---|---|---|
| 0 | 1734.05 | 9372.94 |
| 20 | 1729.11 | 9352.88 |
| 40 | 1724.16 | 9332.82 |
| 60 | 1719.22 | 9312.77 |
| 80 | 1714.27 | 9292.71 |
| 100 | 1709.32 | 9272.65 |

Also, Table 3 shows the efficiency wind energy on the performance of the MES. In this case, the wind speed rate is changed to 20%, 50%, and 80% of the base case and the operating cost and carbon emission are reported in Table 3. When the wind speed rate is less than 100%, the generation of wind turbine is reduced compared to the base case. Therefore, the MES should supply the required electricity by the main grid and other energy sources. Due to the fuel consumption of these resources, it increases the operating cost and carbon emission.

Table 3: Operating cost and carbon emission in different wind speed rate

| Wind speed rate (%) | Cost ($) | Carbon emission (kg) |
|---|---|---|
| 20 | 1793.25 | 9779.74 |
| 50 | 1780.35 | 9678.65 |
| 80 | 1737.75 | 9425.69 |
| 100 | 1709.32 | 9272.65 |

Also, Table 4 shows the performance of the MES in the emergency condition. In the emergency condition, the outpour power of renewable energy sources (PV and wind energy) is curtailed. The numerical results show that

Table 4: Operating cost and carbon emission in normal and emergency condition

| | Cost ($) | Carbon emission (kg) |
|---|---|---|
| Normal condition | 1709.32 | 9272.65 |
| Emergency condition | 1818.17 | 9880.04 |

According to Table 4, in the emergency condition, the operation cost of the MES is increased 6.37% and reaches from $ 1709.32 to $ 1818.17. Also, the emergency condition increases the carbon emission from 9272.65 kg to 9880.04 kg. In the emergency condition, the MES increases the imported electricity from the main grid to compensate the RES shortage. Therefore, it increases the operating cost and carbon emission. Table 5 shows the effect of DR programs on the performance of the proposed model. The simulation results demonstrated that when the electrical and thermal DR programs are implemented, the operating cost of the MES reduces from $ 1752.70 to $ 1709.33. By implementing DR programs, the MES can shift the electrical and thermal loads from peak hours to off-peak hours. Since the electricity prices during off-peak hours are lower than during peak hours, the DR programs reduce the operating cost.

Table 5: Operating cost and carbon emission with/without DR programs

| Case study | Cost ($) | Carbon emission (kg) |
|---|---|---|
| No electrical and thermal DR | 1752.70 | 9272.653 |
| With electrical and thermal DR | 1709.33 | 9272.653 |
| Improvement (%) | 2.47 | 0 |

Table 6 ranks the Pareto solutions by other multi-attribute decision making approaches as well as TOPSIS and SAW methods. The ranking results show that using the SAW and TOPSIS methods, P3 and P4 are simultaneously selected as the top option. In P3 and P4, the emission of the greenhouse gases is 9446.339 kg, which is 173.68 kg higher than the emission level of the proposed MAUT method.

Table 6: Ranking of Pareto solutions using SAW, TOPSIS, and MAUT

| Options | Cost ($) | Emission (kg) | MAUT | TOPSIS | SAW |
|---|---|---|---|---|---|
| P1 | 1673.87 | 9740.947 | 6 | 3 | 3 |
| P2 | 1674.55 | 9705.717 | 5 | 2 | 2 |
| P3 | 1686.61 | 9446.339 | 3 | 1 | 1 |
| P4 | 1686.61 | 9446.339 | 3 | 1 | 1 |
| P5 | 1709.33 | 9272.653 | 1 | 4 | 4 |
| P6 | 1709.33 | 9272.653 | 1 | 4 | 4 |
| P7 | 1709.33 | 9272.653 | 1 | 4 | 4 |
| P8 | 1710.16 | 9271.236 | 2 | 5 | 5 |
| P9 | 1721.07 | 9259.374 | 4 | 6 | 6 |
| P10 | 1869.88 | 9181.783 | 7 | 7 | 7 |
| P11 | 1941.44 | 9180.715 | 8 | 8 | 8 |

## 5 Conclusion

This paper proposes a multi-objective economic and sustainable operation for the integrated energy systems. The proposed structure incorporates the cooling section with the heating and electrical sections to create a flexible and reliable scheduling. The proposed model is developed using normalized weighted sum approach, the Shannon entropy method and multi-attribute utility theory approach to simultaneously minimize the total cost and carbon emission. The proposed model is tested on both normal and emergency condition with renewable generation curtailment. The numerical results show that proposed model decreases the operating cost and carbon emission in the normal condition by 6.37 % and 6.55 %, respectively compared to the emergency condition. In future work, a multi-layer framework will be presented to improve the power quality indices of the multi-energy system. Also, the impact of network reconfiguration on the operating cost of the system will be studied.

## Funding

This work is based upon research funded by Iran National Science Foundation (INSF) under project No 40504370.

## Nomenclature

| Parameters | Description |
|---|---|
| $A^{pv}$ | Surface area for solar panel |
| $B^{pv}$ | Efficiency of PV |
| $C_t^{demand}$ | Cooling demand |
| $C_{e,dr}^{down}$ | Incentive rate for power reduction in EDR |
| $C_{e,dr}^{up}$ | Incentive rate of power increasing in EDR |
| $C_{h,dr}^{down}$ | Incentive rate of power reduction in TDR |
| $C_{h,dr}^{up}$ | Incentive rate of power increasing in TDR. |
| $COP^{ISC}$ | Coefficients performance of ISC |
| $COP^{EC}$ | Coefficients performance of electric chiller |
| $COP^{AC}$ | Coefficients performance of absorption chiller |
| $D_t$ | Electrical load in MES |
| $g$ | Gravity of the earth |
| $G_{\max}^{boiler}$ | Maximum input gas to boiler |
| $G_{\max}^{chp}$ | Maximum input gas to CHP |
| $G_{\max}^{DG}$ | Maximum input gas to gas turbine |
| $H_t^{demand}$ | Heat demand of MES |
| $H^{AC,\max}$ | Maximum input heat to AC |
| $H_{\max}^{boiler}$ | Upper bound of generated heat by boiler |
| $I_{t,s}^{pv}$ | Sun radiation |
| $LHV$ | Natural gas low heat value |
| $N^{pv,mpt}$ | Upper limit of temperature coefficient |
| $P^{\max,grid}$ | Maximum bound for electricity trading with grid |
| $P^{h,\max}$ | Maximum capacity hof heat pipe |
| $P_i^{ch,\max}$ | Upper limit of charging power in electrical or thermal energy storage systems |
| $P_i^{disch,\max}$ | Maximum discharging power limits for electrical or thermal energy storage system |
| $P^{r,wt}$ | Nominal capacity of Vestas V25/200 wind turbine |
| $P^{EC,\max}$ | Maximum input electricity to electric chiller |
| $P_{\max}^{gas}$ | Maximum limit of input natural gas to integrated energy system |
| $S_i^{down}$ | Demand response participation level for load reduction |
| $S_i^{up}$ | Demand response participation level for load expansion |
| $SoC_i^{\min}$ | Minimum allowable SoC for energy storage systems |
| $SoC_i^{\max}$ | Maximum allowable SoC for energy storage systems |
| $T^{pv,c}$ | Reference temperature |
| $T_t^{pv,out}$ | Ambient temperature |
| $U_{em}^{g}$ | Carbon footprint per unit of grid electricity |
| $U_{em}^{chp}$ | Carbon footprint per unit of CHP |
| $U_{em}^{boiler}$ | Carbon footprint per unit of boiler |
| $U_{em}^{DG}$ | Carbon footprint per unit of gas turbine |
| $V^{ci,wt}$ | Cut-in speed |
| $V^{co,wt}$ | Cut-out speed |
| $V^{rr,wt}$ | Rated speed |
| $V_{t,s}^{ac,wt}$ | Wind velocity at time $t$ under scenario $s$ |
| $\eta^{i,ch}$ | Efficiency during charging of energy storage systems |
| $\eta^{i,disch}$ | Efficiency during discharging of energy storage systems |
| $\eta^{e,chp}$ | Electrical efficiency of the CHP unit |
| $\eta^{h,chp}$ | Thermal efficiency of the CHP unit |
| $\eta^{boiler}$ | Thermal efficiency of the boiler |

| | |
|---|---|
| $\eta^{DG}$ | Electrical efficiency of the gas turbine |
| $\pi_t^{Grid}$ | Electricity tariff |
| $\lambda_t^{g}$ | Natural gas tariff |
| Variables | |
| $C_t^{ec}$ | Cooling generation of EC |
| $C_t^{ac}$ | Cooling generation of AC |
| $Cost^{Grid}$ | Main grid cost |
| $Cost^{CHP}$ | Generation cost of CHP |
| $Cost^{boiler}$ | Generation cost of boiler |
| $Cost^{DG}$ | Generation cost of gas turbine |
| $Cost^{EDR}$ | Cost of electric DR |
| $Cost^{HDR}$ | Cost of thermal DR |
| $E_{i,t}^{ch}$ | Binary indicator for charging of battery |
| $E_{i,t}^{disch}$ | Binary indicator for discharging of battery |
| $G_t^{chp}$ | Input natural gas to CHP |
| $G_t^{boiler}$ | Input natural gas to boiler |
| $G_t^{DG}$ | Input natural gas to gas turbine |
| $H_t^{boiler}$ | Heat production of boiler |
| $H_t^{AC}$ | Input heat to AC |
| $P_{c,t}^{disch}$ | Output cooling of ISC |
| $P_t^{Grid}$ | Trading energy with main grid |
| $P_t^{e,chp}$ | CHP electricity production |
| $P_t^{h,chp}$ | CHP heat production |
| $P_t^{DG}$ | Generation of gas turbine |
| $P_t^{ISC}$ | Input electricity by ice storage conditioner |
| $P_t^{EC}$ | Input electricity by electric chiller |
| $P_{i,t}^{down}$ | Reduced power of the MES in DR |
| $P_{i,t}^{up}$ | Increased power of the MES in DR |
| $P_{i,t}^{ch}$ | Charging electricity of battery energy |
| $P_{i,t}^{disch}$ | Discharging electricity of battery energy |
| $P_t^{pv}$ | Electricity generation of PV |
| $P_t^{wt}$ | Electricity generation of wind turbine |
| $SoC_{i,t}$ | Energy level in battery storage |
| $V_{i,t}^{down}$ | Binary variable for down-ward electricity |
| $V_{i,t}^{up}$ | Binary variable for up-ward electricity |

## Disclosure of Potential Conflicts of Interest

The Authors declare that there is no conflict of interest

## Reference

[1] Wang, Jianxiao, Haiwang Zhong, Ziming Ma, Qing Xia, and Chongqing Kang. "Review and prospect of integrated demand response in the multi-energy system." *Applied Energy*, vol. 202, 2017, 772-782, doi.org/10.1016/j.apenergy.2017.05.150.

[2] Yao, Ruiqiu, Yukun Hu, and Liz Varga. "Applications of agent-based methods in multi-energy Systems-A systematic literature review." Energies, vol. 16, no. 5, 2023, p. 2456, doi.org/10.3390/en16052456.

[3] Pastore, Lorenzo Mario. "Sector Coupling and Flexibility Measures in Distributed Renewable Energy Systems: A Comprehensive Review." *Sustainability*, vol. 18, no. 1, 2026, p. 437, doi.org/10.3390/su18010437.

[4] Abba, Ilaria, Alessio La Bella, Stefano Paolo Corgnati, and Edoardo Corsetti. "Assessing flexibility in networked multi-energy systems: A modelling and simulation-based approach." *Energy Reports*, vol. 11, 2024, pp. 384-393, doi.org/10.1016/j.egyr.2023.11.049.

[5] Dou, Zhenlan, Chunyan Zhang, Wei Wang, Dan Wang, Qiqi Zhang, Yanxing Cai, and Ruitian Fan. "Review on key technologies and typical applications of multi-station integrated energy systems." Global Energy Interconnection, vol. 5, no. 3, 2022, pp. 309-327, doi.org/10.1016/j.gloei.2022.06.009.

[6] Liu, Mengke, Manfeng Li, Guofeng Zhou, Juncheng Yang, Linin Zhang, Wei Yang, and Panpan Li. "Optimization and Comparative Analysis of Operating Modes in a Multi-Energy Complementary System Using NSGA-III Algorithm." *Energy*, vol. 355, 2026, 141171, doi.org/10.1016/j.energy.2026.141171.

[7] Jiang, Runhua, Weijia Tang, and Xiaoping Yang. "Performance analysis and optimization of a novel multi-energy storage system for combined cooling, heating and power coupled with advanced compressed air energy storage system." *Applied Thermal Engineering*, vol. 295, 2026, 130702, doi.org/10.1016/j.applthermaleng.2026.130702.

[8] Liang, Kunfeng, Xiaozhe Yang, Haoyuan Chen, Chenguang Zhang, Bin Chen, Xiangqi Gao, and Tieying Yin. "Multi-objective optimization of direct cooling thermal management system for battery energy storage systems." *Journal of Energy Storage*, vol. 166, 2026, 121970, doi.org/10.1016/j.est.2026.121970.

[9] Cao, Baosen, Pengcheng Cai, Chuanbo Wen, and Peilei Feng. "Robust coordinated scheduling of multi-integrated energy systems with user aggregators and electric vehicle charging stations: A Nash-Stackelberg game approach." *Journal of Energy Storage*, vol. 166, 2026, 122430, doi.org/10.1016/j.est.2026.122430.

[10] Ya-Jun LengRui Li, "Economic optimization of integrated energy systems under multiple uncertainties: A multi-timescale scheduling framework driven by wind power forecasting and responses to its errors", *Sustainable Energy, Grids and Networks*, vol. 46, 2026, doi.org /102276, 10.1016/j.segan.2026.102276.

[11] Bayat, Ali, Mohammad Mohammadi, Behrooz Zaker, and Dariush Keihan Asl. "Risk-aware distributed transactive energy management for multi-area systems with cloud energy storage participation." *Journal of Energy Storage*, vol. 164, 2026, 122205, doi.org/10.1016/j.est.2026.122205.

[12] Zhou, Jianli, Zhemei Ma, Xinya Sun, Zihan Xu, Yiran Ma, and Jiayi Zhao. "Optimal capacity configuration of the wind-solar-hydrogen multi-energy system for green data computing centers: An integrated AI forecasting and improved multi-objective optimization approach." *Journal of Cleaner Production*, vol. 554, 2026, 148096, doi.org/10.1016/j.jclepro.2026.148096.

[13] Karimi, Hamid, and Milad Rahimipour Behbahani. "Tri-layer optimization of coupled water–energy storage under renewable uncertainty." *Journal of Energy Storage*, vol. 137, 2025, 118540, doi.org/10.1016/j.est.2025.118540.

[14] Karimi, Hamid. "Bi-level water and energy nexus of virtual power plant and microgrid systems in distribution systems: A hybrid cooperative & non-cooperative framework." *Electric Power Systems Research*, vol. 251, 2026, 112275, doi.org/10.1016/j.epsr.2025.112275.

[15] Khan, Waqar Ali, Ashkan Pakseresht, Caslon Chua, and Ali Yavari. "Multi-objective optimization of hydrogen-integrated hybrid renewable energy systems using an adaptive evolutionary framework." *International Journal of Hydrogen Energy*, vol. 232, 2026, 155001, doi.org/10.1016/j.ijhydene.2026.155001.

[16] Yin, Erxin, and Xiaoling Cao. "A distributionally robust optimization framework for multi-time scale scheduling of integrated electricity-hydrogen energy system." *Electric Power Systems Research*, vol. 258, 2026, 113112, doi.org/10.1016/j.epsr.2026.113112.

[17] Alharbi, Abdullah M., and Ahmed A. Zaki Diab. "Enhancing off-grid hybrid renewable energy systems through multi-objective optimization with Pareto front analysis." Energy, vol. 351, 2026, 140728, doi.org/10.1016/j.energy.2026.140728.

[18] Zaytoun, Ahmed M., Islam A. Abdul Maksoud, and Sherif I. Rabia. "Multi-objective home energy management system with realistic load classification and multi-source uncertainty modeling: A robust optimization approach." *Journal of Process Control*, vol. 162, 2026, 103722, doi.org/10.1016/j.jprocont.2026.103722.

[19] Masoudi, Mohammad Reza, Mehran Haghighi, and Hamid Reza Sezavar. "Optimization of Energy Hub Performance Using the Improved Particle Swarm Optimization (IPSO) Algorithm for Integrated Energy Systems." *In 2025 12th Iranian Conference on Renewable Energies and Distributed Generation (ICREDG)*, pp. 1-6. IEEE, 2025, 10.1109/ICREDG66184.2025.10966138.

[20] Haghighi, Mehran, Mohammad Reza Masoudi, Hamid Karimi, and Hamid Reza Sezavar. "Stochastic Framework for Smart Home Energy Management: Integrating Demand Response and Renewable Resources Using Improved ABC Algorithm." *In 2025 12th Iranian Conference on Renewable Energies and Distributed Generation (ICREDG)*, pp. 1-6. IEEE, 2025, 10.1109/ICREDG66184.2025.10966090.